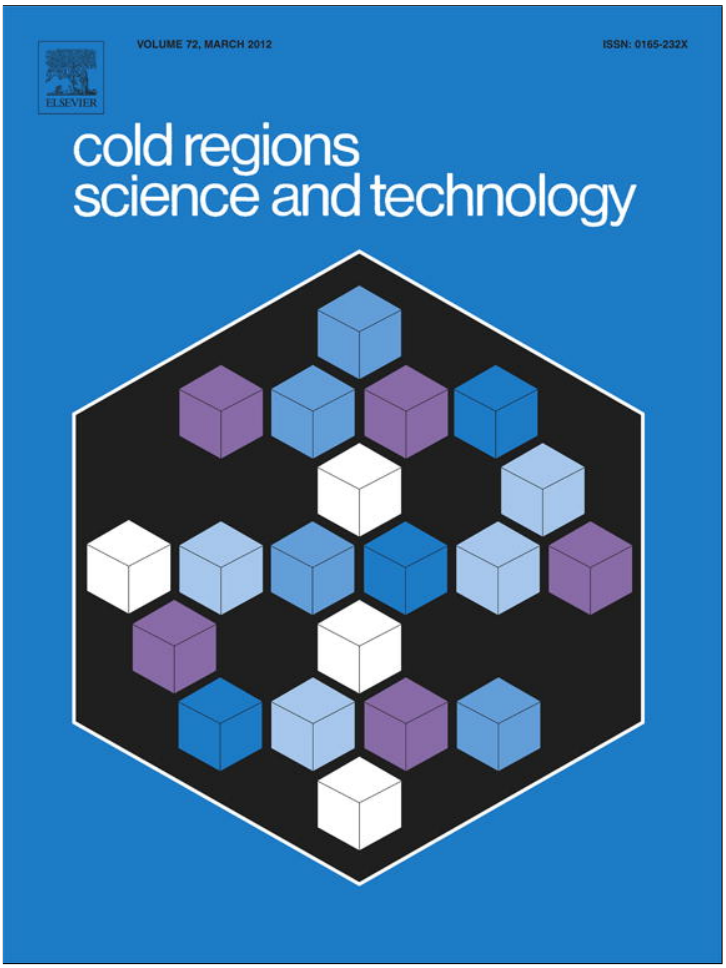

Cold Regions Science and Technology 72 (2012) 23–32

Contents lists available at SciVerse ScienceDirect

Cold Regions Science and Technology

journal homepage: www.elsevier.com/locate/coldregions

Temperature gradient distribution in permafrost active layer, using a prototype of the ground temperature sensor (REMS-MSL) on deception island (Antarctica)

M. Ramos [a,*], M.A. de Pablo [b], E. Sebastian [c], C. Armiens [c], J. Gómez-Elvira [c]

[a] Department of Physics, University of Alcalá, 28871-Alcalá de Henares, Spain
[b] Department of Geology, University of Alcalá, 28871-Alcalá de Henares, Spain
[c] Centro de Astrobiología (CSIC-INTA), Ctra. Ajalvir Km. 4, 28850 Torrejón de Ardoz, Madrid, Spain

ARTICLE INFO

Article history:
Received 1 May 2011
Accepted 27 October 2011

Keywords:
Permafrost
Active layer
Maritime Antarctica
IR temperature sensor

ABSTRACT

Deception Island, an active volcano on South Shetland Archipelago of Antarctica (62°43′S, 60°57′W), is a cold region with harsh, remote and hostile environmental conditions, what could be considered in most aspects such an analog of the Martian surface. The volcanic materials on the surface, the permafrost and active layer existence, and the cold-climate conditions made this region of the Earth a perfect site to test instruments for the future missions to Mars. This is the case of the Ground Temperature Sensor (GTS), based on an infrared radiation (IR) sensor, included into the Rover Environmental Monitoring Station (REMS) instrument on board of the Mars Science Laboratory (MSL) mission of NASA, with that it will measure the Mars surface temperature.

We conducted a summer Antarctic scientific campaign in 2009 on Deception Island in order to test the GTS instrument in the field. That device was placed near other already installed instruments and used to monitor permafrost and active layer thermal evolutions: air, surface and ground temperatures, as well as short and long wave radiation were registered. In brief the main objectives are (1) test in the field and improve the GTS device prototype, and (2) develop a methodology to derive soil gradient temperature in the active layer zone; which could be applied in the MSL mission.

With the obtained data during 2009 campaign, we (a) compared temperatures from GTS versus our Pt100 contact temperature sensors to analyze GTS response accuracy; (b) calculated the active layer thickness using the sinusoidal heat transfer conduction model from soil surface temperature records; and (c) calculated the unfrozen active layer thermal diffusivity.

The main results show that the degree of adjustment between the temperature measurements by to Pt100 contact temperature sensors and the CGT-REMS instrument is high, with a mean error value of below ±0.6 °C although it could reach values of ±5.0 °C due to the heating of the instrument case due to the sun. On the other hand, the calculated active layer thickness was consistent with the direct measures from both; our temperature probes placed in shallow boreholes and mechanical probing. Then, using soil surface temperature data from GTS instrument will be able to establish indirectly the active layer thickness and its thermal structure, what will have important applications for the MSL mission to Mars.

1. Introduction

Compared to other components of the cryosphere, our understanding of Antarctic permafrost and its active layer is poor, especially in relation to its thermal state and evolution, its physical properties, links to pedogenesis, hydrology, geomorphic dynamics and response to global change (Bockheim, 1995; Vieira et al., 2010).

Permafrost, which occupies only 0.36% (49,800 km^2) of the Antarctic region, is present beneath virtually all ice-free terrain, except at the lowest elevations of the maritime Antarctic and sub-Antarctic islands. At these locations, a tightly coupled relationship exists between permafrost and climate variability.

On the volcanic Deception Island, located off the northern tip of the Antarctic Peninsula (maritime Antarctica), the Mean Annual Air Temperature (MAAT) is close to −2 °C, thermal amplitude is low (10 °C monthly mean deviations) and summer mean air temperatures (December to March) are above 0 °C. Permafrost thermal behavior and distribution is mainly influenced by present climatic trends. In addition, this region is located at the approximate limit for the formation or maintenance of permafrost (Ramos et al., 2007).

Changes in the soil thermal regime in response to climate variability directly affect the thickness of the active layer and permafrost temperature. Experimental control of the mechanical and thermal parameters

* Corresponding author. Tel.: +34 1 8854917.
E-mail addresses: miguel.ramos@uah.es (M. Ramos), miguelangel.depablo@uah.es (M.A. de Pablo), sebastianme@inta.es (E. Sebastian), armiensac@inta.es (C. Armiens), gomezej@inta.es (J. Gómez-Elvira).

0165-232X/$ – see front matter © 2011 Elsevier B.V. All rights reserved.
doi:10.1016/j.coldregions.2011.10.012

that define the state of the active layer (maximum depth, temporal evolution of the thermal gradient, snow variability at the soil surface) is necessary to effectively study the impact of regional climate change on permafrost dynamics.

On the other hand due to its present climatic characteristics, Mars is susceptible to the extensive presence of permafrost (Carr, 2006). The study of Martian permafrost could help us to understand the connection between its climate and the soil surface energy balance, which might house microbial life in the same way as terrestrial permafrost.

As a result of previous NASA missions, it is well-known that the average planet surface temperature on Mars is −53 °C, but that temperature varies widely over the course of a Martian day, from −128 °C during the polar night to 27 °C on the equator at midday at the closest point in its orbit around the Sun, with diurnal amplitudes of up to (80 °C, 100 °C). These thermal cycles induce the presence of a thin active layer (millimeters) and a very thick permafrost table (kilometers deep). Much more recent measurements taken by Phoenix mission (May 25th 2008) indicate that Martian regolith temperatures (polar latitudes) range from −92 °C to 20 °C. Additionally, Mars undergoes very extreme active layer temperature gradients above the permafrost and between the ground surface and the atmosphere, temperature gradient values of 40 °C (Smith et al., 2004).

This huge variation in diurnal temperature has a dramatic effect on static stability and hence on the dynamics of the Martian planetary boundary layer. The thermal structure and dynamics of the atmosphere are strongly influenced by the exchange of moisture, heat, mass, and momentum between the permafrost active layer and the Mars atmosphere.

Retrieval of the in-situ surface temperature of Mars is essential to develop environmental models of coupling between the Martian atmosphere-surface boundary layer and ground permafrost (Kreslavsky et al., 2008; Ramos et al., 2008a, 2008b).

From a technical point of view, there are two main methods for performing in-situ Martian surface ground temperature measurements. The first is the use of contact sensors placed a few millimeters below the surface, for example, the NetLander ATMospheric Instrument System (ATMIS) (Polkko et al., 2000) or the Thermal Electrical Conductivity Probe (TECP) contained in the Phoenix Microscopy Electrochemistry and Conductivity Analyzer (MECA) instrument (Zent et al., 2009). Despite their simplicity, it is not always possible to perform these direct soil contact measurements with temperature probes due to mission restrictions, and this is the case for the Rover Environmental Monitoring Station (REMS) instrument on the Mars Science Laboratory (MSL-NASA) mission.

Practical problems due to use of direct soil contact temperature probes include the thermal influence of the probe when deploying the sensor on the ground until it reaches the thermal equilibrium, and the existence of a thin layer of dust over the rocky surface of Mars, which could generate temperature gradients between the surface and the first few millimeters of subsurface, altering the measurement. One alternative to measure soil temperature would be the use of contactless sensors, using Infrared Radiation (IR) spectrometers and radiometers as pyrometers (Sebastian et al., 2010).

Pyrometers are devoted for measuring temperature of bodies, integrating the IR energy coming from them. In general, measuring temperature using IR techniques is more complex than using contact sensors due to the existence of problems associated with the physical measurement procedure. Uncertainty in its IR emissivity (ε) is perhaps the most important of them.

The infrared radiation emitted by Martian surface depends mainly on two factors: (1) the real surface temperature of the focused area and (2) the average emissivity (ε) of the ground, or, what is the same, its capacity to emit IR energy coming from the environment.

Assuming that the Martian ground IR reflectivity is equal to ($r = 1 - \varepsilon$), the expression of the ground radiated heat power is obtained as the sum of the emitted and reflected powers: P radiated = P emitted + P reflected, i.e., [P radiated = ε A E ground + $(1 - \varepsilon)$ E environment], where A is the area of the ground, and E is the heat flux power calculated based on Plank's law and the temperature of the ground and the environment. Therefore, the estimation of ground temperature depends on the environmental heat flux power exchange and ground emissivity.

Typical emissivity values of Martian soils from 6 to 25 μm wavelength vary between 0.9 and 0.99 (Kieffer et al., 1972), introducing significant uncertainty in regard to the power emitted and that reflected by the ground. Thus, in order to achieve a high degree of accuracy in surface temperature measurements, the value of soil emissivity must be estimated or measured. This explains the need for specific studies of IR reflectance properties associated with different types of Martian superficial materials (e.g. minerals and rocks) (Martín-Redondo et al., 2009).

NASA's Mars Science Laboratory (MSL) is the first mission to include an environmental station (REMS), placed on the rover of the mission (Curiosity), and will have a mission duration of one Martian year to enable a study of the completed Martian seasons (Baerg et al., 2010; MSL, 2010). Its launch is scheduled for the fall of 2011. REMS has been developed by the Spanish Center for Astrobiology (CAB-CSIC-INTA) in collaboration with the European Aeronautic Defence and Space Company (EADS-Crisa), the Polytechnic University of Catalunya, the Finnish Meteorological Institute, the NASA Ames Research Centre, the University of Michigan, the University of Alcalá and the California Institute of Technology. REMS has been designed for measuring ambient pressure, humidity, wind speed and direction, UV radiation, and air and ground temperatures (Gomez-Elvira et al., 2009). Specifically, the Ground Temperature Sensor (GTS) is a pyrometer designed to measure the temperature of the Martian surface (Sebastian et al., 2010).

The field test was designed to check Ground Thermal Sensor (GTS-REMS) performance and validate the proposed sensor model and its previous laboratory calibration. Several field tests were held in the surroundings of the Spanish Antarctic Stations (Livingston and Deception Islands) (Fig. 1) during the 2008 and 2009 Antarctic campaigns (Esteban et al., 2009). The most interesting campaign, in terms of Martian analogies, was conducted near the Crater Lake area on Deception Island, where instruments were installed in January 2009 (22/01/2009 to 31/01/2009), and this paper will focus on this experiment. Therefore in January 2009, an engineering model of the GTS was deployed in Antarctica in the surroundings of the Spanish Antarctic Station "Gabriel de Castilla" on Deception Island an active volcano located in the South Shetland archipelago, Maritime Antarctica (62°43′S, 60°57′W). This site was chosen because it represents a remote and hostile environment with harsh environmental conditions and permafrost with a maximum active layer thickness of about 33 ± 5 cm (multiannual mean value, 2006 to 2010) (Ramos et al., 2010a). The soil is formed from volcanic ash and pyroclastic materials, in some sites; there is embedded snow and ice forming discontinuous lenses at variable deeps. In some respects, this location could be considered an analog of Mars (Esteban et al., 2009). The GTS measurements were compared against those taken by standard and calibrated measurement devices which had been installed in order to continuously measure the active layer dynamics of the permafrost, as part of the international program, Circumpolar Active Layer Monitoring South (CALM-South) (Nelson and Shiklomanov, 2010).

This study had two main objectives:

- To validate the GTS infrared sensor and its response accuracy in a harsh, remote and hostile environment by comparing the data it obtained from ground temperature measurements on the surface and in the permafrost active layer with those obtained by standard contact sensors.
- To develop an indirect method that permits us to obtain information about the temperature distribution in the unfrozen active layer zone

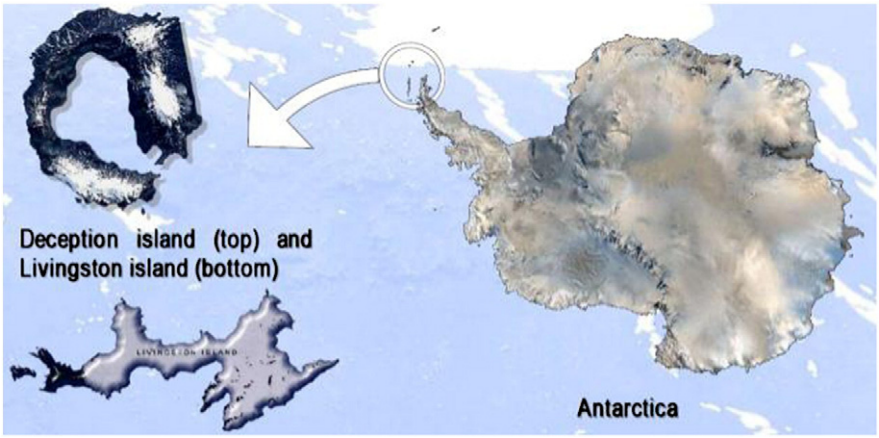

Fig. 1. Location of the study area on Deception Island (South Shetlands Islands, Maritime Antarctic, 62°43′S, 60°57′W). Maps taken from the SCAR (Scientific Committee of Antarctic Research) web site.

based only on soil surface temperature measures and will enable us to study sub-surface temperatures on Mars by measuring directly the soil surface temperatures with the GTS-REMS-MSL device.

2. Study area

Due to its volcanic activity with recent volcanic events (1967, 1969 and 1970), Deception Island (South Shetland Islands, Maritime Antarctic, 62°43′S, 60°57′W) (Fig. 1) is interesting as regards to its permafrost distribution and related processes (Smellie et al., 2002). Interactions between frequency of eruptions, climate, snow cover and permafrost are complex, this produces a stratigraphy with a mix of pyroclastic material, volcanic ashes, ice lenses and a permafrost layer. The ground temperature in Deception Island is not only influenced by climatic conditions, but also by a high geothermal heat flux caused by the volcanic activity on this island (Ramos et al., 1989a). Then, the first meters of the ground, influenced by the cold-maritime climate is marked by the presence of permafrost and its active layer, however, due to the geothermal flux from the volcano and its soil moisture characteristics, the permafrost on Deception Island is shallower than on other nearby islands (Ramos et al., 2007).

The climate at sea level is cold-maritime, with frequent summer rainfall in low-lying areas and a moderate annual temperature range (King and Turner, 1997). The climate reflects the strong influence of the circum-Antarctic low-pressure system. Meteorological conditions in summer are dominated by the continuous influence of polar frontal systems (Styszynska, 2004). Relative humidity is very high, with average values ranging from 80 to 90%. Long term data from different stations on King George Island (South Shetland Archipelago) show the Mean Annual Air Temperature (MAAT) to be approximately −1.6 °C near sea level and the annual precipitation to be about 500 mm of water equivalent. Other regional air temperature data taken at different meteorological stations around Deception Island reflect a MAAT ranging between −3.2 °C and −1.6 °C with an average MAAT value of −2.6 °C (Hauck et al., 2007). From April to November, average daily temperatures generally stay below 0 °C, whilst from December to March they generally rise above this temperature. The annual meteorological data describe two climate cycles corresponding to the annual cycle of soil freezing and thawing (Ramos et al., 2010b).

The CALM-S site on Deception Islands comprised flat terrain with volcanic and pyroclastic fragments on the surfaces and was installed near Crater Lake at 112 m.a.s.l. during the summer of 2006 Antarctic campaign. Although very porous, the soil has an interstitial water content, as much as 2.7% (by weight), such as measured by desiccation method (Ramos et al., 1989B). Soils (Cryosoils), due to the volcanic nature of the materials are slightly acidic (about pH ≈ 5.5) (Greenfield, 1992) and not developed because it formed from pyroclastic materials and ashes from the 1970 eruption. Locally, the soils are slightly colonized by mosses and lichens. Geophysical techniques like electrical resistivity and acoustic propagation and mechanical measurements made by drilling deep boreholes or probing by means of a drill, estimate the active layer thickness and indicate that the permafrost layer is thin, varying between 3 m and 25 m thick, with maximum active-layer thickness (ALT) of around 33 ± 5 cm (multi annual mean value measured by probing at the end of the summer seasons, 2006 to 2010) (Ramos et al., 2007; Ramos et al., 2010a).

3. Experimental method and instrumentation

The GTS-REMS field test site on Deception Island was located at the CALM-S site. Following the CALM-S protocol the GTS-REMS study site is placed in a parcel of 1 ha (100 m × 100 m) in size, which was subdivided into a grid of 10 m × 10 m cells for measuring active layer depth. In the nodes of this grid active layer depth was determined using the mechanical probing method with a manual drill at the end of the summer season (Ramos et al., 2007). Also we implemented an air temperature sensor (Pt-100, Tinytalk, Orion) mounted on a mast at 1.60 m above the surface and protected by a solar radiation shield, a snow layer monitoring system was based on the near soil surface temperature evolution that would complement the mechanical probing and ground temperature systems which were placed in shallow boreholes (100 cm deep) (Table 1). All sensors in these experiences are i-Button (by Maxim http://www.maxim-ic.com/products/ibutton/).

The GTS-REMS is a lightweight, low-power and low-cost pyrometer for measuring the Martian surface temperature. The GTS works by receiving the IR energy radiated by the ground surface, and has a temperature range of between −123 °C and 27 °C. Designed in accordance with REMS scientific requirements, the GTS aims to achieve an accuracy of ±5 °C and a resolution of 0.1 °C (Sebastian et al., 2010). The GTS is mounted on one of the REMS booms (Sebastian et al., 2010), positioned on the NASA/MSL Rover mast at a height of 1.6 m (Fig. 2).

The GTS Antarctic engineering model and its amplification electronics were housed inside a protective casing placed in a horizontal position on the left side of the mast (Fig. 3). The GTS faced the ground at the bottom of the protective casing, at an approximate height of 1.5 m above the surface, giving a field of view of 0.86 m in diameter. The GTS engineering model used for the field test included a thermopile in the 8–14 μm band and a flight calibration plate.

Fig. 3 shows the different components of the GTS Antarctic experiment. On the upper part of the mast, an air temperature sensor (Vaisala Termo-hygrometer, HMP 45A) was housed inside a solar radiation shield (note that on Mars, the REMS will also provide air temperature measurements), whilst the data acquisition system, including battery (Yuasa 12 V/24 Ah) and solar panel (TGM500 12 V

Table 1
Characteristics of the instruments used in the field test experiment.

Sensor	Parameter	Range	Accuracy
2 x Pt100 plates	Soil surface temperature	−80 °C to 600 °C	±0.1 °C
(CNR1) Kipp and Zonen	Solar short wave incoming (DOWN) and reflecting (UP)	0 to 1000 W/m^2	5%
(CNR1) Kipp and Zonnen	Infrared radiation down (coming from atmosphere) and up (coming from soil surface)	−250 to 250 W/m^2	10%
Pt 100 and H(%)	Air temperature	−80 °C to 600 °C	±0.1 °C
Vaisala HMP45A	Relative humidity	0 to 100%	5%
iButton (DS1921L) sensor chain. MAXIM	Ground temperatures	−40 °C to +85 °C	±0.5 °C (0.06 °C resolution)
Battery (Yuasa 12 V/24 Ah)	Power supplied	12 V output	
Solar panel. (TGM-500 12 V (AS))	Power supplied	5 V input 12 V output	
Data logger. Grant 4F16.			

(AS)), was mounted on the lower part of the mast (Table 1). To compare the data products retrieved from GTS measurements (GTS device casing, left part of the mast, Fig. 3), the surface soil temperature was also monitored by means of two different standard instruments: a calibrated Kipp and Zonen CNR1 net radiometer or pyrgeometer (right part of the mast), and two contact temperature probes, based on a RTD (Pt100), and mounted in the exact center of square aluminum with high thermal diffusion plates (10 cm × 10 cm × 0.5 cm) (Table 1). The CNR1 net radiometer, mounted approximately 1.5 m above the ground and facing the ground, was based on a thermopile, as is the GTS, and its measurement band ranged from 5 μm to 50 μm. The surface plate sensors were buried, within the field of view of the GTS, at approximately 0.5 cm below the surface.

A Grant 4F16 data logger was used for the sampling and recording system, which, in addition to the amplified thermopile signal, stored the internal resistance of the thermopile and calibration plate Pt100 temperature sensors and the previously described sensors used for the field test. The sampling rate was every 5 min.

Close to the GTS-REMS installation node (2, 2) of the CALM site grid, ground temperature and its temporal evolution at different depths were also measured, using iButton sensors placed in shallow boreholes 100 cm deep. Sensors were distributed as follows: 2.5; 5.0; 10.0; 20.0; 40.0; 70.0 and 100.0 cm beneath ground level, reaching the permafrost table. This chain of temperature sensors was used to record data for two different experimental periods. In the first period, data was recorded every 3 h between 22/01/2009 (18:00 GMT) and 28/01/2009 (17:00 GMT), whilst in the second period it was recorded every hour between 28/01/2009 (17:00 GMT) and 31/01/2009 (12:00 GMT). The sensor placed 40 cm deep started to record data after 28/01/2009 (17:00 GMT).

GTS-REMS data were processed to transform the effective infrared radiation balance to surface temperatures using the energy balance model proposed by Sebastian et al. (2010). Taking into account the emissivity values previously analyzed in the laboratory using soil samples collected in the study area, soil emissivity was 0.97 (Martín-

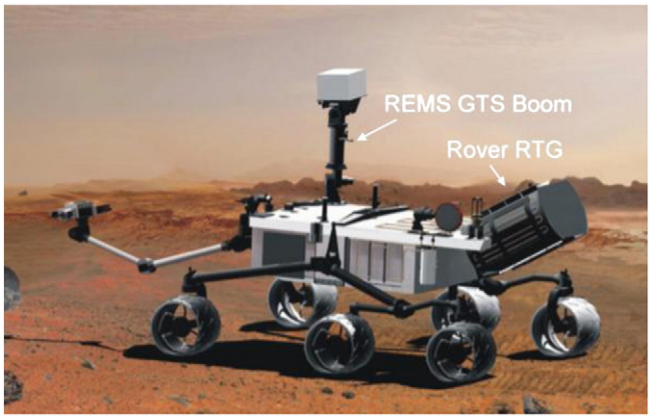

Fig. 2. Recreation of the NASA MSL *Curiosity* Rover on Mars. Picture taken from the MSL (Mars Science Laboratory) web site.

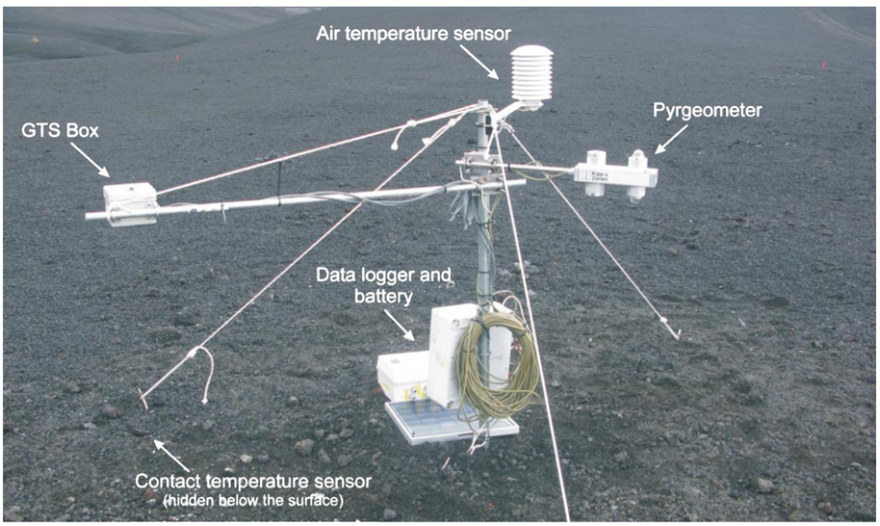

Fig. 3. Deployment of the REMS GTS field test at the CALM-S site, located near the Crater Lake on Deception Island at 112 m.a.s.l., on flat terrain with volcanic debris and ashes on the surface.

Table 2
Statistical values of the meteorological parameters measured at the "Gabriel de Castilla" Station (15 m.a.s.l) during the experimental period (22 to 31 January, 2009).

	Air humidity (%)	Air temperature (°C)	Wind speed (m/s)	Atmospheric pressure (kPa)
	5(%)	±0.1 °C	±0.2(m/s)	±2(kPa)
Mean	88	2.8	5.5	984
Maximum	96	6.6	18.6	991
minimum	61	0.4	0	970
SD Deviation	5	1.0	3.6	4.5

Redondo et al., 2009) and effective atmospheric emissivity was considered 0.92 (Sherwood, 1981).

In addition, local meteorological parameters (air speed and direction, air humidity and temperature, solar radiation and precipitation) were available, having been registered by the meteorological station sited near the "Gabriel de Castilla" Antarctic Spanish Station (15 m.a.s.l.) on Deception Island.

4. Data processing and results

During the experimental period (22 to 31 January, 2009) on Deception Island, the weather was windy (mainly in the daytime), attaining peak wind speed values of 18 m/s with a North West component. Air temperature was between 0 °C and 5 °C and air humidity was quite constant at 85%. Atmospheric pressure at sea level followed a downward trend throughout this period (990 kPa to 975 kPa) (Table 2).

On January 22 and 23, approximately 3 cm of snow fell in the study area, partially covering the soil surface for 24 h. Fig. 4 shows the direct and reflected short wave radiation and the albedo measured in the Crater Lake experiment. The characteristic albedo value (in the range 0.3 to 3 μm) was 0.43 during the period of snow cover, and 0.04 for the pyroclastic surface (without snow cover).

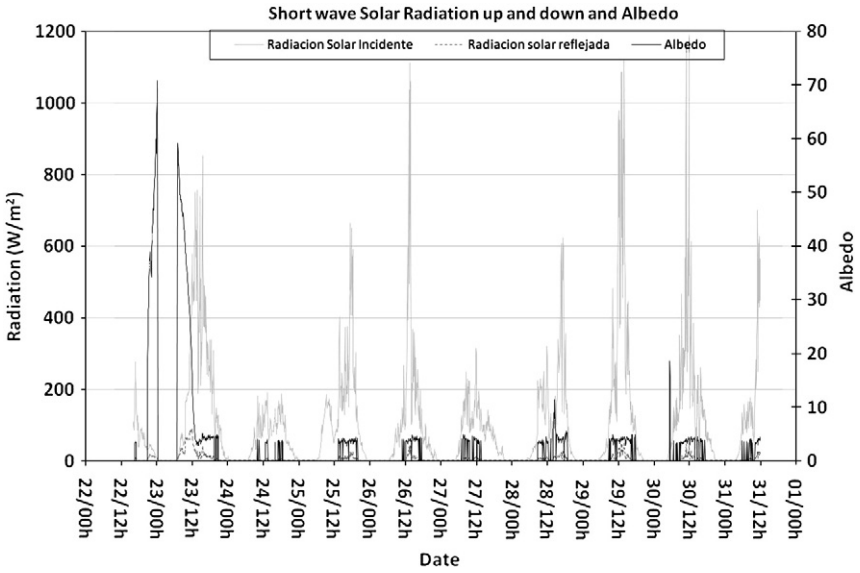

Fig. 4. Direct and reflected short wave radiation and the albedo measured during the "Crater Lake" experiment.

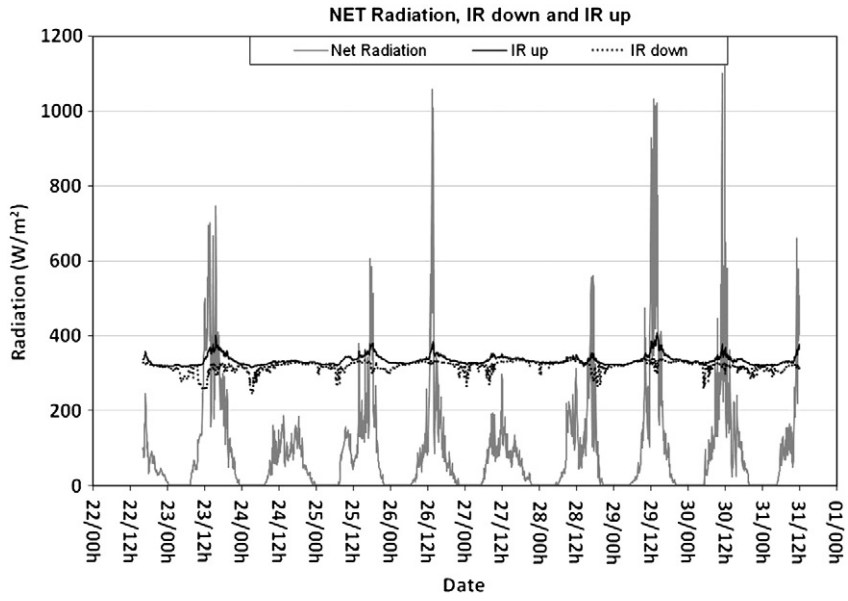

Fig. 5. Infrared Earth radiation UP and DOWN and net radiation values during the experimental period.

Table 3
Main components of the accumulative short and long wave radiation balance on the soil surface at Crater Lake (112 m.a.s.l.) during the experimental period (22 January; 16 h GMT to 31 January; 12 h GMT, 2009) measured by the meteorological Kipp and Zonnen CNR1 net radiometer.

	Solar short wave DOWN	Solar short wave UP	Solar short wave	Long wave UP	Long wave DOWN	Long wave	Net rad.
Balance (MJ/m^2)	80 ± 5	3.0 ± 0.2	77 ± 4	250 ± 25	240 ± 25	-10 ± 1	67 ± 5

The four components of earth and solar radiation were measured directly at Crater Lake by means of a meteorological Kipp and Zonnen CNR1 pyrgeometer as a part of the experiment (Fig. 5). The radiation energy balance during the experimental period was studied at the soil surface test site. Short wave radiation was measured in the spectral range of 0.3 to 3 μm coming to the sun and sky (DOWN short wave radiation) and the reflected one coming to the soil surface (UP short wave radiation) the accumulative addition in the study period is the balance of each component (DOWN and UP). The solar balance will be the difference between DOWN and UP components and represent the net solar energy accumulated by the soil surface. Respects to the long wave radiation were measured in the spectral range of 5 to 50 μm, the radiation coming to the sky (DOWN) and emitted by the soil surface (UP). Long wave balance will be again the difference between DOWN and UP components. Finally the NET radiation balance in the study period will be the accumulated energy coming to the short and long wave components. Table 3 shows the main components of this radiation balance. The period of collecting data for all radiation parameters was 5 min.

4.1. Surface temperature

Soil surface temperature measure was analyzed using those records obtained by the meteorological Kipp and Zonnen CNR1 net radiometer, the data measured by Pt100 plates in direct contact with the soil, located just below the infrared sensors (left bottom in Fig. 3) and using GTS-REMS infrared detector. The comparison between soil surface temperatures registered by different instruments (contact plates or infrared radiometer sensors CNR1 and GTS) constituted a technique for identifying differences in soil surface temperatures as recorded under working field conditions by different instruments. Some of the little differences observed between contact and infrared measurements (mean $T_{plate} - T_{soilGTS} \approx 0.6$ °C) may have been due to the thermal inertia of the thermal plate that is covered by a few millimeters of the soil, in contrast to the infrared method that measured just the surface temperature by means of the indirect pyrometric color method. In addition, indirect temperatures measured by the infrared method depended on thermal emissivities (soil and atmosphere) and the algorithm applied whilst contact plates are placed just below the soil surface.

Main experimental parameter values for day and night periods during the experience are shown in Figs. 6 and 7. Error values were given as the differences between the mean soil surface temperature values registered by the Pt100 soil contact plates and the indirect soil surface temperature measured by the infrared sensors (GTS and CNR1) during the study periods (Fig. 6). Short and long (infrared) wave radiations were calculated by temporal integration of these radiation components during 6 hour time periods starting from 21/01/2009, 16:00 to the end of the experiment on 31/01/2009 (Fig. 7).

The data in Figs. 6 and 7 correspond to sunny daytime (0, 12, 24… hour) and night-time (6, 18, 30…hour) periods. The mean error between the CNR1 meteorological sensor and the contact plates (mean value over the complete measured period; 1.9 °C) was greater than the mean error obtained using the GTS-REMS sensor and the contact plates (mean value over the complete measured period; 0.6 °C) for all periods (day/night) (Fig. 6). In addition, dispersion of these differences was also greater during daytime periods, mean day dispersion error of 0.8 °C for the T_{plates}–$T_{soilGTS}$ mean error values in contrast with 0.3 °C for night. At night, dispersion values were lower as seen in the differences between the contact plates and the infrared GTS and CNR1 sensors, indicating that thermopile temperature stability was better at night than during sunny day.

These differences between the soil surface temperatures obtained by GTS in contrast with CNR1 sensors can be explained by the fact that the GTS-REMS sensor applies the complex algorithm of Sebastian et al. (2010) using emissivity values measured from field samples. In contrast, the CNR1 meteorological sensor uses Stefan's law of black body emissivity ($\varepsilon = 1$).

However, in most cases the mean difference between the soil surface temperatures registered, regardless of the instrument used,

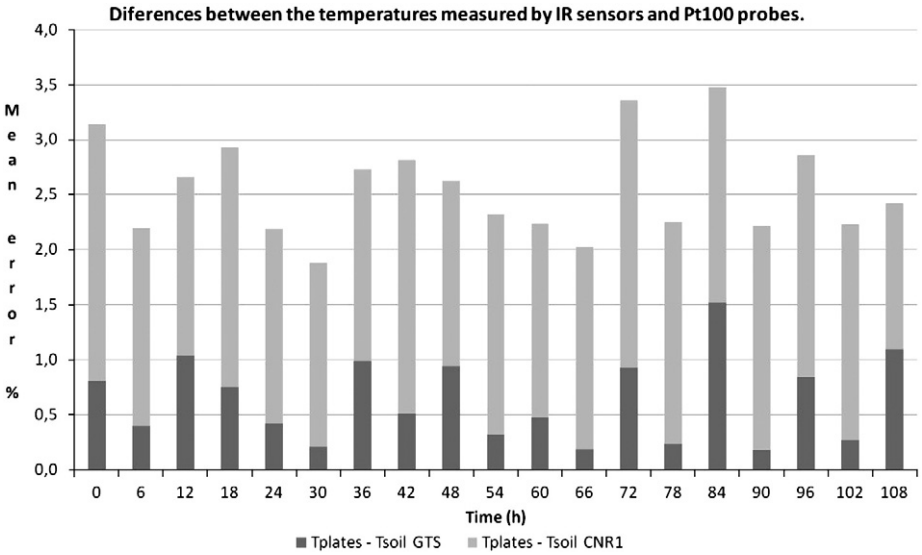

Fig. 6. Values of the error that is considered the mean (each 6 hour periods) of the differences between soil surface temperature measurements registered by Pt100 contact plates and these measured by the IR sensors GTS or the CRN1, during the experiment that started in 21/01/2009, 16:00. Tplates (soil surface temperature measured by the contact plates), Tsoil GTS (estimated soil surface temperature measured by the GTS-REMS sensor), Tsoil CNR1 (estimated soil surface temperature measured by the CNR1 meteorological sensor).

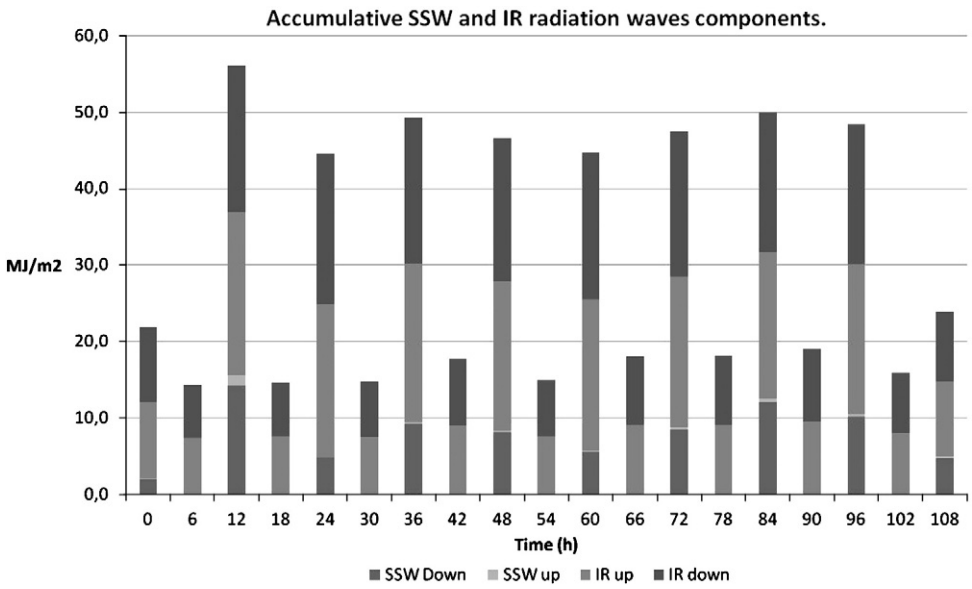

Fig. 7. Values of the accumulative short SSW (Solar Short wave Radiation) and long wave IR (Infrared Radiation), radiation calculated each 6 h during the experiment that started in 21/01/2009, 16:00.

was less than ±5 °C, which is the maximum admissible deviation for the GTS-REMS mission design (Sebastian et al., 2010). Values very rarely exceeded the ±5 °C limit, except in a few isolated instances as a result of the casing receiving solar radiation producing a heat from the casing that altered the measurement registered by the GTS device in contrast with that registered by the CNR1 solar radiometer, which has a thermal inertial design to avoid these perturbations (Fig. 8).

4.2. Ground temperatures

Fig. 9 shows the temporal evolution of ground temperature for all the sensors at different depths, it can be seen that thermal evolution presented periodic behavior in all positions; signals had a common daily period of approximately 24 h. Thermal amplitude also varied with depth; greater amplitude values were recorded by the soil surface contact plate sensors, whilst lower amplitude values were recorded below the active layer (between 20 and 40 cm for this experiment). In these cases, amplitude was zero due to the phase change process that occurs at these depths. Furthermore, a signal delay, relative to surface temperature evolution, was observed, which increased with depth. All these effects are related to the heat transfer process of a periodic signal by conduction and depend on mean thermal diffusivity, since the active layer zone thaws completely in the summer and the phase change does not occur in this period.

Temperature evolution data was analyzed applying the periodic heat transfer conduction approach and using quasi-stationary sinusoidal signal propagation (Ayra, 1988). In this case, attenuation of thermal amplitude with depth shows the following exponential dependency:

$$A(x) = A_0 e^{-x/d} \quad (1)$$

$$d = \sqrt{P\alpha/\pi} \quad (2)$$

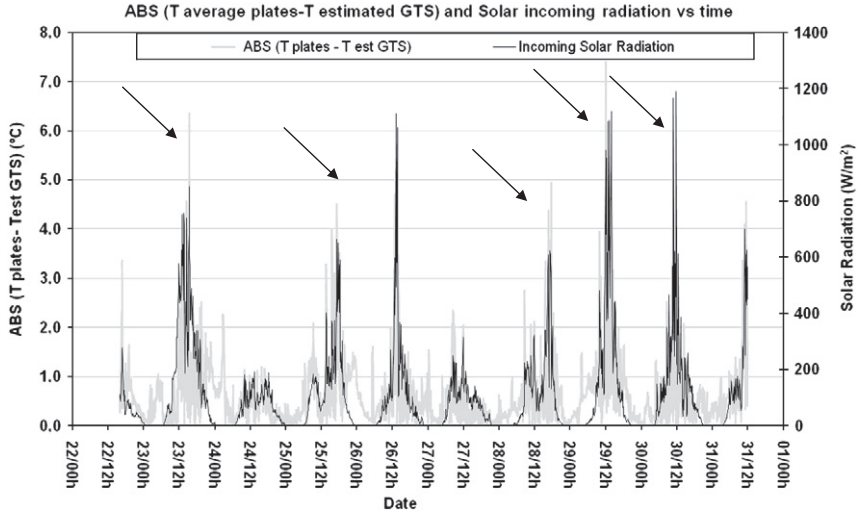

Fig. 8. Differences between soil surface temperatures measured by contact plates and those measured by the infrared GTS-REMS sensor are shown in the graph, together with the evolution of short wave solar radiation during the experimental period. In a few isolated instances as a result of the casing receiving solar radiation producing a heat from the casing that altered the measurement registered by the GTS device in contrast with that registered by the CNR1 solar radiometer, which has a thermal inertial design to avoid these perturbations (see the arrows in the graph).

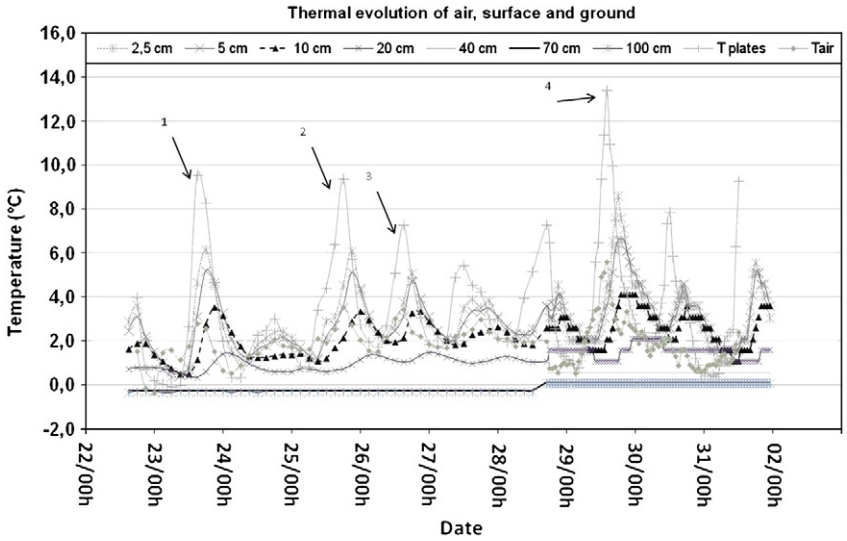

Fig. 9. Time evolution of the air, soil surface and ground temperatures inside the 100 cm borehole drilled close to the experience in "Crater Lake" experimental site, during the measuring period. The numerated peak corresponds to the study of periodic events.

Table 4
Values for thermal amplitude and delay of periodic signal propagation at the different depths in the active layer zone during the experimental period for the selected signals shown in Fig. 9.

Date Peak n°	Surface A (°C) ±0.25°C Delay (h)	0.5 cm A (°C) ±0.25°C Delay (h)	2.5 cm A (°C) ±0.25°C Delay (h)	5.0 cm A (°C) ±0.25°C Delay (h)	10.0 cm A (°C) ±0.25°C Delay (h)	20.0 cm A (°C) ±0.25°C Delay (h)	Air (°C) ±0.1°C
23/01/09	5.7	4.6	2.9	2.4	1.5	0.4	2.8
Peak 1	0	0	3	3	6	9	
25/01/09	7.2	5.2	2.5	2.0	1.1	0.4	3.6
Peak 2	0	0	3	3	6	9	
26/01/09	2.8	2.5	1.5	1.3	0.7	0.2	3.4
Peak 3	0	0	3	3	6	6	
29/01/09	7.2	6.9	3.5	2.3	1.3	0.5	5.6
Peak 4	0	2	6	7	9	12	

where A(x) is the thermal amplitude (°C) at x-depth (m). A_0 is the thermal amplitude (°C) on the surface. P is the signal period (s) and α is soil thermal diffusivity (m^2/s).

We applied the heat transfer hypothesis to the study of four events, selecting the most significant periodic signal behaviors from among the soil surface and ground temperature sensors, as shown in Fig. 9. Records of thermal amplitude (semi-differences between maximum and minimum values over a complete period) were extracted from the data for each depth and the time when maximum values were attained (relative to the soil surface temperature peak). All these parameters are given in Table 4.

Thermal amplitude A(x) versus depth x plots (Figs. 10 and 11), show a good exponential fit for all the study events, confirming the periodic signal hypothesis of conduction heat transfer. Table 5 shows the exponential fit and the inverse value of the exponential coefficient, d (cm), and the R^2-parameter, which represents the adjusted correlation value.

The standard value of the depth at which thermal amplitude was zero (Ayra, 1988), for this signal (24-hour period), was considered approximately $3d = 23 \pm 3$ cm. That corresponds to the measure of the active layer depth that was verified by mechanical probing across the CALM site during the experience (Ramos et al., 2008b).

4.3. Thermal diffusivity

In addition, value for apparent thermal diffusivity in the unfrozen active layer was estimated using Eq. (2). Considering the mean value found by analysis of the thermal evolution signal d (m) and P (s), we found: $\alpha \approx (2.2 \pm 0.5)\ 10^{-7}\ m^2/s$, which is consistent with the range

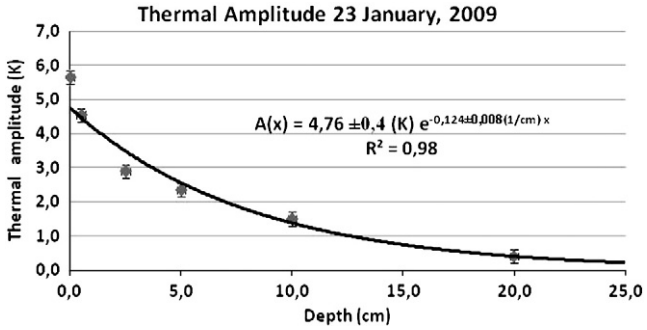

Fig. 10. Thermal amplitude on 23 January, 2009 versus depth and exponential fit.

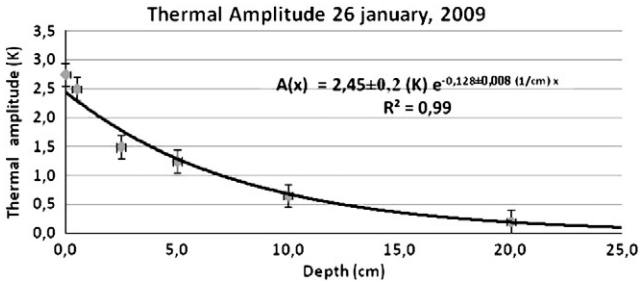

Fig. 11. Thermal amplitude on 26 January, 2009 versus depth and exponential fit.

of values obtained by direct analysis of the thermodynamic parameters of soils in the Crater Lake area (Ramos et al., 1989b).

5. Conclusions

A detailed description of the Antarctic experiment based on a field design of a contactless ground temperature sensor for Mars (GTS-REMS) has been given. The sensor was field tested in the surroundings of the "Gabriel de Castilla" Spanish Antarctic Station on Deception Island, at Crater Lake, a site with presence of permafrost in volcanic pyroclastic soil.

In conclusion:

- The performance of the GTS-REMS sensor was evaluated through comparison with a commercial Kipp and Zonnen CNR1 net radiometer and with direct contact soil surface thermal monitoring. The degree of adjustment with the CGT-REMS, choosing suitable soil and atmospheric emissivities and using the color pyrometry method, was high, with a mean error value of below ± 0.6 °C. In all cases, comparisons with soil surface contact sensors fell within the range of ± 5 °C for both types of radiometer.
- The thermal gradient observed in the GTS casing was due to incoming solar short wave radiation, which heated the casing and the system, requiring a period of stabilization that could induce errors in data recording.
- Analysis of soil gradient temperatures has provided information about thermal daily characteristics in the soil, such as signal period and the parameter for attenuation of temperature wave propagation.
- Active layer thickness was calculated with the aid of temperature recording data using the sinusoidal heat transfer conduction model in soil, and was consistent with the systematic measures performed at this experimental station by direct mechanical probing.
- Using periodic soil surface temperature signals and knowing soil apparent thermal diffusivity value in the unfrozen active layer zone, it would be possible to calculate indirectly the mean of the periodic heat transfer solution: the temporal evolution of the soil and its active layer depth.
- In the future, the Mars Science Laboratory mission (NASA) will provide soil surface temperature data obtained by the GTS-REMS sensor. These data will be analyzed in order to obtain information on the thickness of the soil active layer on Mars and the implications of soil thermodynamics for the possible presence of life.

Table 5
Adjusted exponential coefficients,1/d (1/cm), A_0 (°C) and R^2 parameter.

Date Peak no	1/d (1/cm)	A_0 (°C)	R^2
23/01/09 Peak 1	0.124 ± 0.008	4.76 ± 0.4	0.98
25/01/09 Peak 2	0.133 ± 0.02	4.81 ± 0.8	0.93
26/01/09 Peak 3	0.128 ± 0.008	2.45 ± 0.2	0.99
29/01/09 Peak 4	0.129 ± 0.01	5.56 ± 0.5	0.96

Mean value, $1/d = 0.129 \pm 0.02$ (1/cm).

Acknowledgments

The research was supported by Spanish Antarctic Program by the PERMAPLANET project CTM2009-10165 and REMS project EPS2007-65862. The authors are grateful for the helpful comments of the anonymous reviewers and of the editor on an earlier version of the manuscript.

References

Ayra, S. Pal, 1988. Introduction to Micrometeorology. Academic Press Inc. (ISBN 0-12-064490-8).
Baerg, M., Beck, J., Hulme, S., Lievense, S., Tozzi, E., Viotti, M., Webster, G., 2010. Mars Science Laboratory(Available online:) http://mars.jpl.nasa.gov/msl/overview/2010 (accessed on 25 April 2010).
Bockheim, J.G., 1995. Permafrost distribution in the Southern Circumpolar Region and its relation to the environment: a review and recommendations for further research. Permafrost and Periglacial Processes 6, 27–45.
Carr, M.H., 2006. The Surface of Mars. Cambridge University Press, Nueva York. (ISBN: 978-0-521-47201-0).
Esteban, B., Ramos, M., Sebastián, E., Armiens, C., Gómez-Elvira, J., Cabos, W., de Pablo, M.A., 2009. The Antarctic permafrost as a testbed for REMS (Rover Environmental Monitoring Station—Mars Science Laboratory). Proceedings of EGU2009-1292. General Assembly, Vienna, Austria.
Gomez-Elvira, J., Castañer, L., Lepinette, A., Moreno, J., Polko, J., Sebastián, E., Torres, J., Zorzano, 2009. M.P. REMS, an Instrument for Mars Science Laboratory Rover. Proceedings of the 40th Lunar and Planetary Science, The Woodlands, TX, USA, 23–27 March 2009.
Greenfield, L.F., 1992. Retention of precipitation nitrogen by Antarctic mosses, lichens and fellfield soils. Antarctic Science 4 (2), 205–206.
Hauck, C., Blanco, J., Gruber, S., Vieira, G., Ramos, M., 2007. Geophysical identification of permafrost in Livingston Island, Maritime Antarctica. Journal of Geophysical Research 112, F02S19. doi:10.1029/2006JF000544 (ISSN 0148-0227).
Kieffer, H., Neugebauer, G., Munch, G., Chase, J.R., Miner, E., 1972. Infrared thermal mapping experiment: the Viking Mars orbiter. Icarus 16, 47–56.
King, J.C., Turner, J., 1997. Antarctic Meteorology and Climatology. Cambridge University Press, Cambridge;, pp. 114–120.
Kreslavsky, M.A., Heada, J.W., Marchantc, D.R., 2008. Periods of active permafrost layer formation during the geological history of Mars: implications for circum-polar and mid-latitude surface processes. Planetary and Space Science 56, 289–302.
Martín-Redondo, M.P., Sebastian, E., Fernández Sanpedro, M.T., Armiens, C., Gómez-Elvira, J., Martinez-Frias, J., 2009. FTIR reflectance of selected minerals and their mixtures: implications for the ground temperature-sensor monitoring on Mars surface environment (NASA/MSL-Rover Environmental Monitoring Station). Journal of Environmental Monitoring 11, 1428–1432.
MSL Team. NASA's, 2009. Mars Science Laboratory(Available online:) http://marsoweb.nas.nasa.gov/landingsites/msl/memoranda/MSL_overview_LS.pdf2009(accessed on 25 April 2010).
Nelson, F.E., Shiklomanov, N.I., 2010. The Circumpolar Active Layer Monitoring Network—CALM III (2009–2014): long-term observations on the Climate-Active Layer-Permafrost system. In: Blanco, J.J., Ramos, M., de Pablo, M.A. (Eds.), Proceedings of II Iberian Conference of the International Permafrost Association Periglacial, Environments, Permafrost and Climate Variability. UAH, pp. 9–15 (ISBN: 978-84-9138-885-5).
Polkko, J., Harri, A.M., Siili, T., Angrilli, F., Calcutt, S., Crisp, D., Larsen, S., Pommereau, J.P., Stoppato, P., Lehto, A., Malique, C., Tillman, J.E., 2000. The NetLander atmospheric instrument system (ATMIS): description and performance assessment. Planetary and Space Science 48, 1407–1420.
Ramos, M., Ortiz, R., Diez-Gil, J.L., Viramonte, J.G., 1989a. Anomalías Térmicas y Balance del Flujo disipado en la Isla Decepción. Shetlands del Sur. Actas del III Simposio de Estudios Antárticos. CICYT, Madrid, pp. 203–219 (ISBN.-84 369 1903 3).
Ramos, M., Domínguez, M., Ortiz, R., 1989b. Caracterización de algunos parámetros Termodinámicos del suelo del volcán Decepción. Actas del III Simposio de Estudios Antárticos. CICYT, Madrid, pp. 220–223 (ISBN.-84 369 1903 3).
Ramos, M., Vieira, G., Gruber, S., Blanco, J.J., Hauck, C., Hidalgo, M.A., Tomé, D., Neves, M., Trindade, A., 2007. Permafrost and active layer monitoring in the Maritime Antarctic: preliminary results from CALM sites on Livingston and Deception Islands. U.S. Geological Survey and The National Academies; USGS OF-2007-1047, Short Research Paper 070. doi:10.3133/of2007-1047.srp070.
Ramos, M., Gómez-Elvira, J., Sebastian, E., Martín, J., Armiens, C., Blanco, J.J., de Pablo, M.A., Tomé, D., 2008a. Antarctic experience on a permafrost region to test REMS (Rover Environmental Monitoring Station—Mars Science Laboratory) sensors. Proceedings of EGU General Assembly, Vienna, Austria, 13–18 April 2008; Volume 10, EGU2008-A-01434.
Ramos, M., Vieira, G., Gruber, S., Blanco, J.J., Hauck, C., Hidalgo, M.A., Tome, D., Neves, M., Trindade, A., 2008b. Permafrost and active layer monitoring in the Maritime Antarctic: preliminary results from CALM sites on Livingston and Deception

Islands. U.S. Geological Survey and The National Academies;USGS OF-2007–1047, Short Research Paper 070. doi:10.3133/of2007-1047srp070.

Ramos, M., Vieira, G., Guilichinski, D., de Pablo, M.A., 2010a. Nuevas estaciones de medida del régimen térmico del permafrost en el área de "Crater Lake. Isla Decepción (Antártida). Resultados preliminares". In: Blanco, J.J., Ramos, M., de Pablo, M.A. (Eds.), Proceedings of II Iberian Conference of the International Permafrost Association Periglacial, environments, permafrost and climate variability. UAH, pp. 93–109 (ISBN: 978-84-9138-885-5).

Ramos, M., Vieira, G., Gruber, S., De Pablo, M.A. y, Correia, A., 2010b. Estado térmico del permafrost en el monte Reina Sofía, primer año de registro continuo.Isla Livingston (Antártida). In: Blanco, J.J., Ramos, M., de Pablo, M.A. (Eds.), Proceedings of II Iberian Conference of the International Permafrost Association Periglacial, environments, permafrost and climate variability. UAH, pp. 79–92 (ISBN: 978-84-9138-885-5).

Sebastian, E., Armiens, C., Gomez-Elvira, J., Zorzano, M.P., Martinez-Frias, J., Esteban, B., Ramos, M., 2010. The Rover Environmental Monitoring Station Ground Temperature Sensor: a pyrometer for measuring ground temperature on Mars. SENSORS 10 (10), 9211–9231. doi:10.3390/s101009211 (ISSN: 1424-8220).

Sherwood, B.I., 1981. A set of equations for full spectrum and 8–14 μm and 10.5–12.5 μm thermal radiation from cloudless skies. Water Resources Research 17, 295–304.

Smellie, J.L., López-Martínez, J., Headland, R.K., Hernández-Cifuentes, Maestro, A., Miller, I.L., Rey, J., Serrano, E., Somoza, L., Thomson, J.W., 2002. Geology and geomorphology of Deception Island (78 pp.) BAS GEOMAP Series. British Antarctic Survey, Cambridge (Sheets 6-A and 6-B, 1:25,000).

Smith, M.D., Wolff, M.J., Lemmon, M.T., Spanovich, N., Banfield, D., Budney, C., Clancy, R.T., Ghosh, A., Landis, G.A., Smith, P., Whitney, B., Christensen, P.R., Squyres, S.W., 2004. First atmospheric science results from the mars exploration rovers Mini.-TES. Science 306, 1750–1753.

Styszynska, A., 2004. The origin of coreless winters in the South Shetlands area (Antarctica). Polish Polar Research 25, 45–66.

Vieira, G., Bockheim, J., Guglielmin, M., Balks, M., Abramov, A., Boelhouwers, J., Cannone, N., Ganzert, L., Gilichinsky, D.A., Gotyachkin, S., Lopez-Martinez, J., Meiklejohn, I., Raffi, R., Ramos, M., Schaefer, C., Serrano, E., Simas, F., Sletten, R., Wagner, D., 2010. Thermal state of permafrost and active-layer monitoring in the Antarctic: advances during the International Polar Year 2007–2009. Permafrost and Periglacial Processes 21 (2), 182–197. doi:10.1002/ppp.685 (ISSN: 1045-6740).

Zent, A.P., Hecht, M.H., Cobos, D.R., Campbell, G.S., Campbell, C.S., Cardell, G., Foote, M.C., Wood, S.E., Mehta, M., 2009. Thermal and Electrical Conductivity Probe (TECP) for Phoenix. Journal of Geophysical Research 114, E00A27.